Modeling Water Vapor and Clouds in an Idealized GCM

Yi Ming * and Isaac M. Held

Geophysical Fluid Dynamics Laboratory/NOAA, Princeton, NJ

* *Corresponding author address:* Yi Ming, Geophysical Fluid Dynamics Laboratory/NOAA, P. O. Box 308, Princeton, NJ 08542.

E-mail: Yi.Ming@noaa.gov

ABSTRACT

This paper introduces an idealized general circulation model (GCM) in which water vapor and clouds are tracked as tracers, but are not allowed to affect circulation either through latent heat release or cloud radiative effects. The cloud scheme includes an explicit treatment of cloud microphysics and diagnoses cloud fraction from a prescribed sub-grid distribution of total water. The model is capable of qualitatively capturing many large-scale features of water vapor and cloud distributions outside of the boundary layer and deep tropics. The subtropical dry zones, mid-latitude storm tracks and upper-tropospheric cirrus are simulated reasonably well. The inclusion of cloud microphysics (namely rain re-evaporation) has a significant effect of moistening the lower troposphere in this model. When being subjected to a uniform fractional increase of saturated water vapor pressure, the model produces little change in cloud fraction. A more realistic perturbation, which considers the non-linearity of the Clausius-Clapeyron relation and spatial structure of CO_2-induced warming, results in a substantial reduction in the free-tropospheric cloud fraction. This is reconciled with an increase of relative humidity by analyzing the probability distributions of both quantities. The implications of these results and the utility of the idealized model for understanding cloud feedback are discussed.

1. Introduction

A complicating factor in simulating and understanding the climatic roles of water vapor (WV) and clouds is their tight coupling with circulation, posing a major bottleneck in narrowing the uncertainty of cloud feedback (Bony et al. 2015). This motivates us to construct a model of passive WV and clouds, meaning that both are advected as tracers that do not feed back on circulation either through latent heat release or through cloud radiative effects (CRE). Such a model can be thought of as part of a model hierarchy designed for elucidating the complex interplay between moisture and circulation (Held 2005).

Besides cloud feedback, this model may help address what factors have the potential to control the distribution of tropospheric WV. Sun and Lindzen (1993) postulated that tropical relative humidity (RH) was influenced significantly by cloud microphysics, in particular re-evaporation of hydrometeors. This view was later countered by a body of literature collectively known as the advection-condensation theory (Salathé and Hartmann 1997; Pierrehumbert et al. 2007, and references therein), which put more emphasis on circulation and succeeded in reproducing some gross features of RH. These studies typically used simple saturation adjustment (i.e. WV in excess of saturation being removed instantaneously as surface precipitation), and did not include explicit cloud microphysics. Models with passive WV and clouds would allow us to re-evaluate the relative importance of cloud microphysics and circulation in setting tropospheric RH in a self-consistent framework.

2. Model Description and Experimental Design

The model described here is an example of a class of models that can be constructed based on an atmospheric dry dynamical core coupled with a GCM's cloud physics, or with more simplified or more complex versions of the latter. There is no convective parameterization. The large-scale flow is unaffected by the WV and cloud fields. In theory the flow could be stored offline and read into the model as needed but this is typically inconvenient.

Our example of such a model (referred to as the cloud model here) is forced thermally to a prescribed equilibrium temperature profile via Newtonian relaxation, and, as there is no explicit boundary layer parameterization, wind fields are damped by Rayleigh friction near the surface, precisely as in Held and Suarez (1994). Three water tracers are advected: specific humidity, liquid and ice condensates. Surface evaporation is mimicked by nudging RH below $\sim$850 hPa to 100% with a time scale of 30 minutes. The large-scale cloud scheme is the same as implemented in the Geophysical Fluid Dynamics Laboratory (GFDL) HiRAM model (Zhao et al. 2009). Cloud fraction and condensation are diagnosed from grid-mean total water (WV and cloud condensates) using an assumed subgrid-scale distribution, which takes the form of a beta distribution with the width controlled by the grid-mean total water multiplied by a width parameter, just as in Tompkins (2002). The shape parameters p and q in Eq. (7) of Tompkins (2002) are set at 5, resulting in a symmetrical distribution; the width parameter is set at 0.2 in our control simulation. Cloud microphysics is adopted from Rotstayn (1997) and Rotstayn et al. (2000), same as in GFDL AM2 (The GFDL Global Atmospheric Model Development Team 2004) and AM3 models (Donner et al. 2010). This single-moment scheme takes into account the main pathways for transformations between cloud condensates, precipitation formation, and re-evaporation of condensates and precipitation. Condensation (re-evaporation) is assumed not to generate latent heating (cooling), and thus does not affect flow. There are no cloud or WV radiative effects as no explicit radiation is involved. In this sense, WV and clouds are completely passive. Using the cloud scheme from a particular full GCM in this way is a test of concept. Examining a whole variety of microphysical schemes may be of interest in this context, varying from much more idealized schemes, to the schemes used in other GCMs, to bin-microphysical models.

The model analyzed here has a spectral dynamical core with a horizontal resolution of T42, and 20 equally spaced vertical sigma layers. There is no claim that this simulation is converged as horizontal and especially vertical resolution is increased. Studies of the dependence of results such as these on resolution, and the dynamical core more generally, will hopefully be facilitated by this model configuration. The algorithm for tracer advection is identical to that used for passive tracer advection with this spectral dynamical core in the past (e.g. Galewsky et al. 2005; Polvani and Esler 2007). Since it has not been documented in those studies, we describe it in a short appendix.

In an alternative model configuration (referred to as the saturation adjustment model), the cloud scheme is replaced with saturation adjustment. The only water tracer is specific humidity. As any newly formed condensate is assumed to fall out of the air immediately, this model, which is similar to that used in Galewsky et al. (2005), cannot be used to simulate clouds. We perform control simulations with these two models (referred to as CNTL-C and CNTL-SA, respectively). The RH difference between them tells us how the inclusion of the cloud scheme influences the distribution of tropospheric WV. To further separate the influences of cloud macrophysics (partial cloudiness in the cloud model vs. full cloudiness in the saturation adjustment model) and microphysics (present in the cloud model vs. absent from the saturation adjustment model), we design a sensitivity experiment with the cloud model, in which the aforementioed width parameter is lowered to 0.01. This has an effect of allowing for cloud formation only when grid-mean RH essentially reaches 100%, thus switching from zero to full cloudiness (saturation adjustment). This experiment is referred to as NW (Narrower Width). The difference between CNTL-C and NW can be attribute to the change of cloud macrophysics, while the inclusion of cloud microphysics results in the difference between NW and CNTL-SA.

In order to explore the responses of WV and clouds to increased saturated water vapor pressure (e_s), we carry out three perturbation experiments with the default cloud model. In the first one (referred to as UN, UNiform), e_s used in moist physics and diagnosis (e.g. RH) (denoted as e_s^*) is increased uniformly by 14%, regardless of temperature T:

$$e_s^*(T) = 1.14 e_s(T). \tag{1}$$

This is motivated by the commonly held notion that e_s increases with T approximately by 7% K^{-1}, a useful starting point for thinking about the hydrological response to CO_2-induced warming. In this sense, the specified e_s increase represents the thermodynamical effect of a 2 K warming. This, however, is strictly valid only for a temperature range typical of the surface. The second experiment (referred to as TS, Temperature Square) relaxes this restriction by taking into account the temperature-dependence of the Clausius-Clapeyron relation:

$$e_s^*(T) = 1.14 e_s(T) \left(\frac{293}{T} \right)^2 . \tag{2}$$

At 233 K (representative of the upper troposphere), the percentage increase is about 80%, much larger than at the surface. In the third experiment (referred to as TC, Temperature Cubic), we further enhance the temperature-dependence from square to cubic to partially factor in the effect of upper-tropospheric amplification, a consequence of the moist adibatic lapse rate, as well as polar amplification. The resulting expression is

$$e_s^*(T) = 1.14 e_s(T) \left(\frac{293}{T}\right)^3 . \tag{3}$$

This further elevates the percentage increase to about 130% for 233 K. For a surface warming of 2 K, the upper troposphere can be warmer by 5 K in GCMs, which would increase local e_s by about 200%. Therefore, the cubic dependence still likely underestimates the relative change of e_s for the upper troposphere.

In using this procedure to mimic some of the effects of warming, one must keep in mind the several ways in which this cannot capture the effects of warming in comprehensive models. These include the effects of changes in circulation and also the effects of warming on the ice/liquid partitioning in clouds.

3. Results

a. Control Simulations

A measure of the overall hydrological cycle strength, the global-mean precipitation (evaporation) is virtually the same ($\sim$2.4 mm day^{-1}) in CNTL-C and CNTL-SA. Except for small differences in the deep tropics and mid- to high latitudes, the zonal distributions of precipitation and evaporation are also similar (Fig. 1). The precipitation features three distinct peaks in the deep tropics and over the mid-latitude storm tracks, and is outweighed by evaporation by a factor of 4 - 5 in the subtropical dry zones. These results confirm that detailed cloud microphysical treatment is not necessary for simulating the large-scale features of the hydrological cycle in these passive models. This does not necessarily imply that the precipitation distribution is unaffected by cloud microphysical assumptions in comprehensive GCMs due to at least two complicating factors. First, the general circulation in the passive models does not vary with cloud microphysics by design. Second, the hydrological cycle in comprehensive GCMs is constrained by the atmospheric radiative balance, while there exists no such constraint in these passive models. In these models, the strength of the hydrological cycle is controlled by the rate of export of WV out of the saturated boundary layer by the circulation. This is true in more comprehensive models as well, but there is no feedback here between the radiative cooling of the free troposphere with the circulation exporting WV out of the boundary layer.

A comparison with the aqua-planet simulations performed with the comprehensive GCMs in the Aquaplanet Intercomparison Project [Fig. 3 of Blackburn et al. (2013)] suggests that the cloud model captures many gross features of the global RH distribution, including the subtropical dry zones, dry upper troposphere and moist mid- and high latitudes. The RH in the deep tropics (15°S - 15°N) is too high (over 80%) due to the absence of moist convection either parameterized or resolved, which is the main mechanism of tropical dehydration in comprehensive GCMs. For the same reason, the outflow from the tropical ascent is more spread vertically in this model than in the aqua-planet simulations, causing the subtropical dry zones to be placed lower. Similar conclusions can be drawn by comparing with the comprehensive CMIP3 (Coupled Model Intercomparison Project Phase 3) model results [Fig. 1 of Sherwood et al. (2010)]. Replacing saturation adjustment with the cloud scheme tends to moisten the subtropics and mid-latitudes (15° - 60°) by a few percent (in absolute RH) (the lower panel of Fig. 2). The drying of the polar upper troposphere can be attributed partly to the treatment of partial cloudiness in the cloud model as described below.

The total non-evaporation WV tendency is given in Fig. 3. The three local maxima (the deep tropics and mid-latitudes) correspond to the Intertropical Convergence Zone (ITCZ) and storm tracks (the upper panel). Both models generate similar spatial patterns, substantiating that saturation adjustment, as simple as it is, is indeed sufficient for capturing the gross features of precipitation. The biggest differences lie approximately over ∼30° - 60° and between ∼500 and 800 hPa; the WV sink (or the condensate source) is stronger in CNTL-C than in CNTL-SA, coinciding with higher surface precipitation associated with storm tracks in the former.

A decomposition of the tendency in CNTL-C on the microphysical process level confirms that condensation is the dominant sink of WV, and is responsible for the vast majority of precipitation formation (Fig. 4). Ice deposition takes over in the upper troposphere, but is about one order of magnitude smaller than condensation. Rain re-evaporation, which occurs when falling raindrops enter unsaturated air, is a non-negligible source of WV in the subtropical and mid-latitude lower troposphere. A sensitivity experiment with re-evaporation switched off indicates that it is indeed partly responsible for the moistening. (In comparison, cloud liquid re-evaporation is almost negligible, and is not shown.) As another source of WV over the mid-latitudes, snow sublimation is of comparable magnitude, but generally deeper into the atmosphere's interior than re-evaporation.

As described in the previous section, NW is an intermediate case between CNTL-C and CNTL-SA. The upper panel of Fig. 5 shows that the consideration of partial cloudiness tends to decrease simulated RH everywhere by allowing cloud and precipitation to form at a lower RH threshold value. The largest reduction (more than 3%) occurs over the high-latitudes, indicating that the different treatment of subgrid variability is responsible for a similar feature of the RH difference between the two control simulations (the lower panel of Fig. 2). The effect of incorporating cloud microphysics can be isolated by comparing NW with CNTL-SA (the low panel of Fig. 5). It has marked spatial structure, with strong moistening in the lower troposphere (especially over ∼15 - 60°), which is also present in the RH difference between CNTL-C and CNTL-SA. This confirms the significant role of microphysics in modifying lower-tropospheric RH in this model.

Fig. 6 depicts the simulated cloud fields in CNTL-C. The simulated boundary layer clouds are unrealistic due to the lack of a boundary layer scheme, and we view this model's relevance as restricted to the free troposphere. The cloud model is capable of qualitatively reproducing some familiar aspects of the highly inhomogeneous global cloud distribution. In the free troposphere, clouds are most prevalent in the mid- and high latitudes (especially over the storm tracks), where the cloud fraction often exceeds 20% and extends vertically through almost the entire tropospheric column. The tropical upper troposphere (∼100 - 300 hPa) is another place with large cloud fraction. As a reminder, the model used here does not have parameterized or resolved convection. In the subtropical dry zones cloud fraction is generally less than 10%. The transition from cloud liquid to ice follows the freezing line.

b. Perturbation Experiments

We use the cloud model to explore how RH and clouds would vary with increased e_s. The results are given in Fig. 7. A uniform increase of 14% barely causes any change in RH (UN minus CNTL-C, the upper panel); WV increases approximately by the same percentage as e_s. The inherent non-linearity of the Clausius-Clapeyron relation (i.e. the temperature dependence of the fractional increase of e_s per degree of warming) gives rise to appreciable increase of free tropospheric RH, which amounts to more than 1% in the subtropical dry zones and mid-latitude lower troposphere (TS minus CNTL-C, the middle panel). An attempt to take into account the additional effect of upper tropospheric and polar warming (TC minus CNTL-C, the lower panel) amplifies the same pattern seen in TS.

The corresponding changes in cloud fraction are shown in Fig. 8. There is almost no change in UN (the upper panel), consistent with the muted response in RH. Both TS and TC give rise to marked reductions of similar spatial pattern. In the latter experiment, cloud fraction decreases by up to 2% in the subtropical dry zones. The entire free troposphere over $\sim$30° - 50° also undergoes substantial reduction of cloud fraction ($\sim$2%). This trend extends to the high-latitude upper troposphere. The result that cloud fraction decreases despite higher RH is counter-intuitive; they decrease together in comprehensive GCM comparisons (Zelinka et al. 2013). From the perspective of cloud parameterization, the idealized model effectively diagnoses cloud fraction from RH since WV is usually much larger than the cloud condensates.

To better understand the opposing RH and cloud fraction changes, we examine the probability distributions of instantaneous RH and cloud fraction for a domain between 15° and

45°N and between 600 and 700 hPa (Fig. 9). The RH distribution (the upper panel) is reminiscent of that produced with the back trajectory technique [Fig. 6.17 of Pierrehumbert et al. (2007)]. Unlike the specific GCM used in Pierrehumbert et al. (2007), the idealized model, despite being low-resolution, simulates a strong dry spike in the probability distribution of RH. As RH increases, its occurrence becomes less frequent. Only occasionally does RH rise above 80%, the approximate threshold for cloud formation in the default cloud model. The vast majority of the samples are cloud-free (the lower panel). The cloud fraction distribution is relatively flat all the way to ∼80%, but with a distinct bump between 80% and 100%.

In comparison with CNTL-C, the uneven increase of e_s in TC shifts the dry spike in RH toward higher RH, accompanied by a marked increase in probability of intermediate RH (20% to 80%) . At the same time, values higher than 80% become less likely. On balance, the former outweighs the latter, resulting in an increase of the average RH. The lower occurrence of RH greater than 80% explains the reduction in the average cloud fraction. One can rationalize the RH changes using the concept of last saturation (Pierrehumbert et al. 2007). The WV specific humidity (q) of a descending parcel (with its present temperature denoted as T_1) is the same as the saturated specific humidity (q_s) when it last experienced saturation (with its temperature denoted as T_0). Thus, its RH at pressure P_1 can be written as $[e_s(T_0)/e_s(T_1)](P_1/P_0)$, where P_0 is the atmospheric pressure of the parcel when it reaches the last saturation. If one imposes the increase of e_s in the form of Eq. 3, the perturbed RH would be $[e_s(T_0)/e_s(T_1)](P_1/P_0)(T_1/T_0)^3$, which is an increase since T_1 is greater than T_0 for a descending parcel. For an ascending parcel, T_0 is greater than T_1, meaning that RH would become smaller with increased e_s if q is conserved. The assumption of constant q does not hold for precipitating parcels once they are saturated, but the fact that T_0

is greater than T_1 for ascending parcels suggests that larger displacements are needed to achieve saturation, resulting in a decrease in RH on average in these ascending parts of the circulation. Parcels drier (wetter) than ~80% RH are typically associated with descending (ascending) motion, the above analysis help explain why the dry parcels become more humid in the two perturbation experiments with spatial variations, while the opposite occurs to the wet ones. The latter is the underlying cause of reduced cloud fraction. These simulations are missing the effects of the increase in depth of the troposphere with warming that reduces the increase in the temperature of last saturation and therefore damps the increase in RH that would otherwise occur.

Cloud liquid and ice respond largely in opposite directions (Figs. 10 and 11, respectively). Despite higher RH in the lower free troposphere, cloud liquid generally decreases with cloud fraction. In contrast, cloud ice increases at higher altitudes, more consistent with RH change. Note that the temperature used for partitioning condensate into liquid and ice does not change, the upward shift of the freezing line, which is often discussed in the literature, is not an issue here. Thus, it is not straightforward to compare these results with full GCM simulations.

4. Discussion and Conclusions

One can think of the idealized model introduced in this paper as a natural extension of the advection-condensation theory/model that was instrumental for understanding the distribution of tropospheric WV. By decoupling WV and clouds from circulation, the model helps answer to what extent they can be rationalized as being driven by a given circulation.

The advection-condensation theory makes the case that circulation is the dominant factor in shaping the large-scale structure of RH. Given the strong link between RH and clouds (cloud fraction in particular), one probably should not be surprised by how well the idealized model is able to reproduce some of the salient features of the global cloud distribution. This suggests that it may be feasible to study the climatology of certain cloud systems (e.g. frontal and cirrus clouds) in a non-interactive mode.

A main characteristic of full GCM-simulated response to CO_2-induced warming is a widespread reduction of free-tropospheric cloud fraction equatorward of 60° [Fig. 6 of Zelinka et al. (2013)]. This coincides with a reduction of RH [Fig. 2 of Sherwood et al. (2010)], and is usually attributed to circulation changes (namely the poleward shift of storm tracks and the upward expansion of troposphere). It is interesting that the idealized model, when forced cleanly by a purely thermodynamical effect (namely increased saturated water vapor pressure, one of the most robust outcomes of warming), is able to simulate a similar reduction of cloud fraction in the absence of any circulation change. Even more interestingly, the disappearance of clouds is accompanied by an enhancement of average RH. These results are useful for thinking about full GCM-simulated positive cloud feedback. First, although it is reasonable to expect circulation changes to have certain bearings on cloud distribution at the boundaries of circulation regimes, their roles may be somewhat limited within the interiors as warming-induced circulation changes are generally subtle. Second, average RH is not generally a good proxy for cloud fraction as cloud formation is skewed strongly to high RH. Third, the spatial pattern of warming (e.g. upper-tropospheric and polar amplifications) may be effective at altering the probability distribution of both RH and clouds.

Much of the literature on cloud feedback is on low boundary layer clouds (e.g. Zhang et al. 2013). Recent studies highlight the roles of parameterized convection in affecting tropospheric cloud condensates and WV through convective detrainment (Sherwood et al. 2014; Mauritsen and Stevens 2015; Zhao et al. 2016). Because the idealized model does not have boundary layer or cumulus parameterization, its utility for studying low cloud feedback and possible connection with convection is limited. Equipped with an explicit treatment of cloud microphysics, the model, however, is skillful in simulating the subtropical dry zones. Given how tightly linked free-tropospheric RH and boundary layer clouds are, it could prove to be useful for understanding certain aspects of low cloud feedback.

One motivation for suggesting a model with passive WV and clouds in a dry dynamical core is to remove the distinctions in cloud simulations that result from differences in convection schemes in GCMs, allowing a focus on the roles of cloud microphysical and macrophysical (cloud fraction) assumptions. Computations with this class of models may also prove useful in isolating dependencies on the resolution and numerics of the dynamical core arising from the presence of a microphysical package.

In conclusion, we present an idealized model that tracks WV and clouds as tracers, but does not allow them to interact with circulation either through latent heat release or CRE. It can simulate many gross features of WV and cloud distributions in extratropical free tropopshere. The subtropical dry zones, mid-latitude storm tracks and upper-tropospheric cirrus are captured qualitatively in the simulations. It is found that cloud microphysics (namely rain re-evaporation) plays a modest role in moistening the lower troposphere in this model. An uneven increase of saturated water vapor pressure motivated by global warming simulations has a tendency to reduce free-tropospheric cloud fraction, while RH increases.

Acknowledgments.

The authors thank Peter Phillips for help with model setup, and Michelle Frazer for useful discussion. Ming Zhao and Max Popp kindly reviewed an earlier version of the paper.

APPENDIX

Tracer Advection

The dynamical core is a standard spectral core with the prognostic variables vorticity, divergence, temperature, and the logarithm of surface pressure with Simmons-Burridge (Simmons and Burridge 1981) vertical-differencing and with all variables, including the components of the velocities, defined at the same grid points (an A-grid) on a latitude-longitude Gaussian grid. Because the logarithm of surface pressure is the prognostic variable, the model does not conserve mass exactly.

Advecting this model's passive tracers, WV and especially the condensed water phases utilized by the microphysics, with spectral advection would contaminate these fields hopelessly with Gibb's ripples. Instead we use a finite-volume grid point advection scheme. We first write the advection operator in an equivalent "faux flux form" without weighting the velocity by the pressure thickness (i.e., surface pressure):

$$\mathbf{v} \cdot \nabla \xi = \nabla \cdot (\mathbf{v}\xi) - \xi \nabla \cdot \mathbf{v} \tag{A1}$$

The last term is evaluated on the A grid since the spectral model provides the divergence on this grid. The horizontal faux flux-form transport is computed using the finite volume formulation of Lin and Rood (LR) (Lin and Rood 1996). The velocities are fist linearly interpolated to the C grid. The horizontal transport is then evaluated assuming a piecewise linear approximation to the sub-grid distribution of tracer, while the vertical transport uses a piecewise parabolic assumption, with monotonicity limiters as in LR. We also evaluate separately the "integer flux" contribution to the zonal advection, avoiding any time step constraint due to zonal advection, once again as in LR. The latter is necessary for an efficient scheme on the latitude-longitude grid.

The spectral model uses leapfrog time step with filtering to avoid separation of even and odd time steps. The tracer advection is adapted to this framework by advecting the tracer over a leapfrog time of $2\delta t$ and using the same Robert filter on the tracer fields.

This way of incorporating grid point advection into a spectral model has some awkward features but has advantages in simplicity over other approaches, and shares the problem of non-conservation globally. The quality of this formulation is illustrated by the Polvani and Esler (2007) study of transport of tracers during baroclinic life cycles and the Galewsky et al. (2005) analysis of the sources of subtropical WV, both of which use this algorithm.

Our motivation for retaining a spectral core is the exact zonal symmetry of the algorithm, which is an attractive feature for idealized studies such as this in which the model climate should be exactly zonally symmetric in the absence of sampling errors or the (unlikely) non-uniqueness of the climate state. Sensitivity of idealized circulation models carrying a microphysical package to the numerical schemes employed for circulation and for tracer transport, as well as resolution, should be of interest.

REFERENCES

Blackburn, M., et al., 2013: The aqua-planet experiment (APE): Control SST simulation. *J. Meteorol. Soc. Jpn.*, **91A**, 17–56, doi:10.2151/jmsj.2013-A02.

Bony, S., et al., 2015: Clouds, circulation and climate sensitivity. *Nature Geosci.*, **8**, 261–268, doi:10.1038/ngeo2398.

Donner, L. J., et al., 2010: The dynamical core, physical parameterizations, and basic simulation characteristics of the atmospheric component of the GFDL global coupled model CM3. *J. Climate*.

Galewsky, J., A. Sobel, and I. M. Held, 2005: Diagnosis of subtropical humidity dynamics using tracers of last saturation. *J. Atmos. Sci.*, **62**, 3353–3367.

Held, I. M., 2005: The gap between simulation and understanding in climate modeling. *B. Am. Meteorol. Soc.*, **86**, 1609–1614.

Held, I. M. and M. J. Suarez, 1994: A proposal for the intercomparison of the dynamical cores of atmospheric general circulation models. *B. Am. Meteorol. Soc.*, **75**, 1825–1830.

Lin, S.-J. and R. B. Rood, 1996: Multidimensional flux-form semi-lagrangian transport schemes. *Mon. Wea. Rev.*, **124**, 2046–2070.

Mauritsen, T. and B. Stevens, 2015: Missing iris effect as a possible cause of muted hydrological change and high climate sensitivity in models. *Nature Geosci.*, **8**, 346–351, doi:10.1038/ngeo2414.

Pierrehumbert, R. T., H. Brogniez, and R. Roca, 2007: On the relative humidity of the atmosphere. *The Global Circulation of the Atmosphere*, T. Schneider and A. H. Sobel, Eds., Princeton University Press, 143–185.

Polvani, L. M. and J. G. Esler, 2007: Transport and mixing of chemical air masses in idealized baroclinic life cycles. *J. Geophys. Res.*, **112**, doi:10.1029/2007JD008555.

Rotstayn, L. D., 1997: A physically based scheme for the treatment of stratiform clouds and precipitation in large-scale models. I: Description and evaluation of microphysical processes. *Quart. J. Roy. Meteor. Soc.*, **123**, 1227–1282.

Rotstayn, L. D., B. F. Ryan, and J. Katzfey, 2000: A scheme for calculation of the liquid fraction in mixed-phase clouds in large-scale models. *Mon. Wea. Rev.*, **128**, 1070–1088.

Salathé, E. P. and D. L. Hartmann, 1997: A trajectory analysis of tropical upper-tropospheric moisture and convection. *J. Climate*, **10**, 2533–2547.

Sherwood, S. C., S. Bony, and J.-L. Dufresne, 2014: Spread in model climate sensitivity traced to atmospheric convective mixing. *Nature*, **505**, 37–42.

Sherwood, S. C., W. Ingram, Y. Tsushima, M. Satoh, M. Roberts, P. L. Vidale, and P. A. O'Gorman, 2010: Relative humidity changes in a warmer climate. *J. Geophys. Res.*, **115**, doi:10.1029/2009JD012585.

Simmons, A. J. and D. M. Burridge, 1981: An energy and angular-momentum conserving vertical finite-difference scheme and hybrid vertical coordinates. *Mon. Wea. Rev.*, **109**, 758–766.

Sun, D.-Z. and R. S. Lindzen, 1993: Distribution of tropical tropospheric water vapor. *J. Atmos. Sci.*, **50**, 1643–1660.

The GFDL Global Atmospheric Model Development Team, 2004: The new GFDL global atmosphere and land model AM2-LM2: Evaluation with prescribed SST simulations. *J. Climate*, **17**, 4641–4673.

Tompkins, A. M., 2002: A prognostic parameterization for the subgrid-scale variability of water vapor and clouds in large-scale models and its use to diagnose cloud cover. *J. Atmos. Sci.*, **59**, 1917–1942.

Zelinka, M. D., K. E. T. S. A. Klein, T. Andrews, M. J. Webb, J. M. Gregory, and P. M. Forster, 2013: Contributions of different cloud types to feedbacks and rapid adjustments in cmip5. *J. Climate*, **26**, 5007–5027, doi:10.1175/JCLI-D-12-00555.1.

Zhang, M., et al., 2013: CGILS: Results from the first phase of an international project to understand the physical mechanisms of low cloud feedbacks in general circulation models. *J. Adv. Model. Earth Syst.*, **5**, 826–842, doi:10.1002/2013MS000246.

Zhao, M., I. M. Held, and G. A. S.-J. Linand G. A. Vecchi, 2009: Simulations of global hurricane climatology, interannual variability, and response to global warming using a 50-km resolution GCM. *J. Climate*, **22**, 6653–6678.

Zhao, M., et al., 2016: Uncertainty in model climate sensitivity traced to representations of cumulus precipitation microphysics. *J. Climate*, **29**, 543–560.

List of Figures

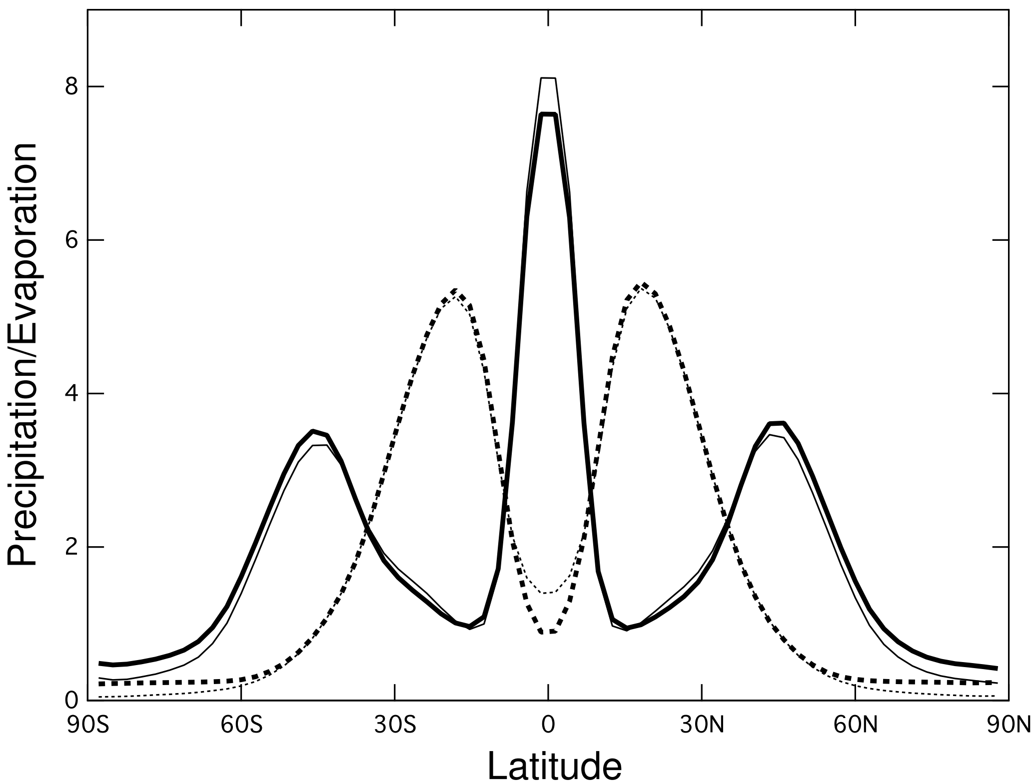

FIG. 1. Zonal-mean precipitation (mm day^{-1}, solid lines) and evaporation (mm day^{-1}, dotted lines) simulated in CNTL-C (thick lines) and in CNTL-SA (thin lines).

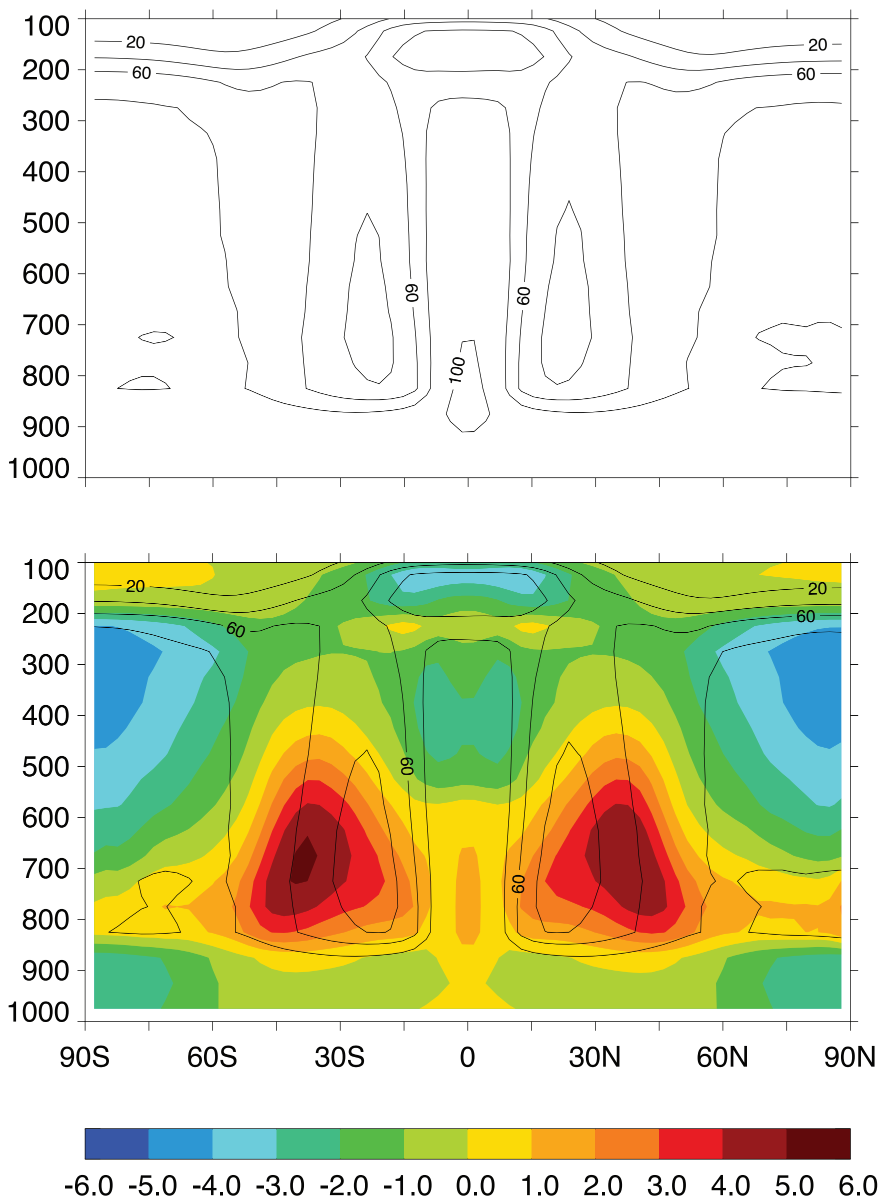

FIG. 2. RH (%) simulated in CNTL-C (contours in the upper panel) and in CNTL-SA (contours in the lower panel). The difference (defined as the former minus the latter throughout this paper) is shown in color shading in the lower panel.

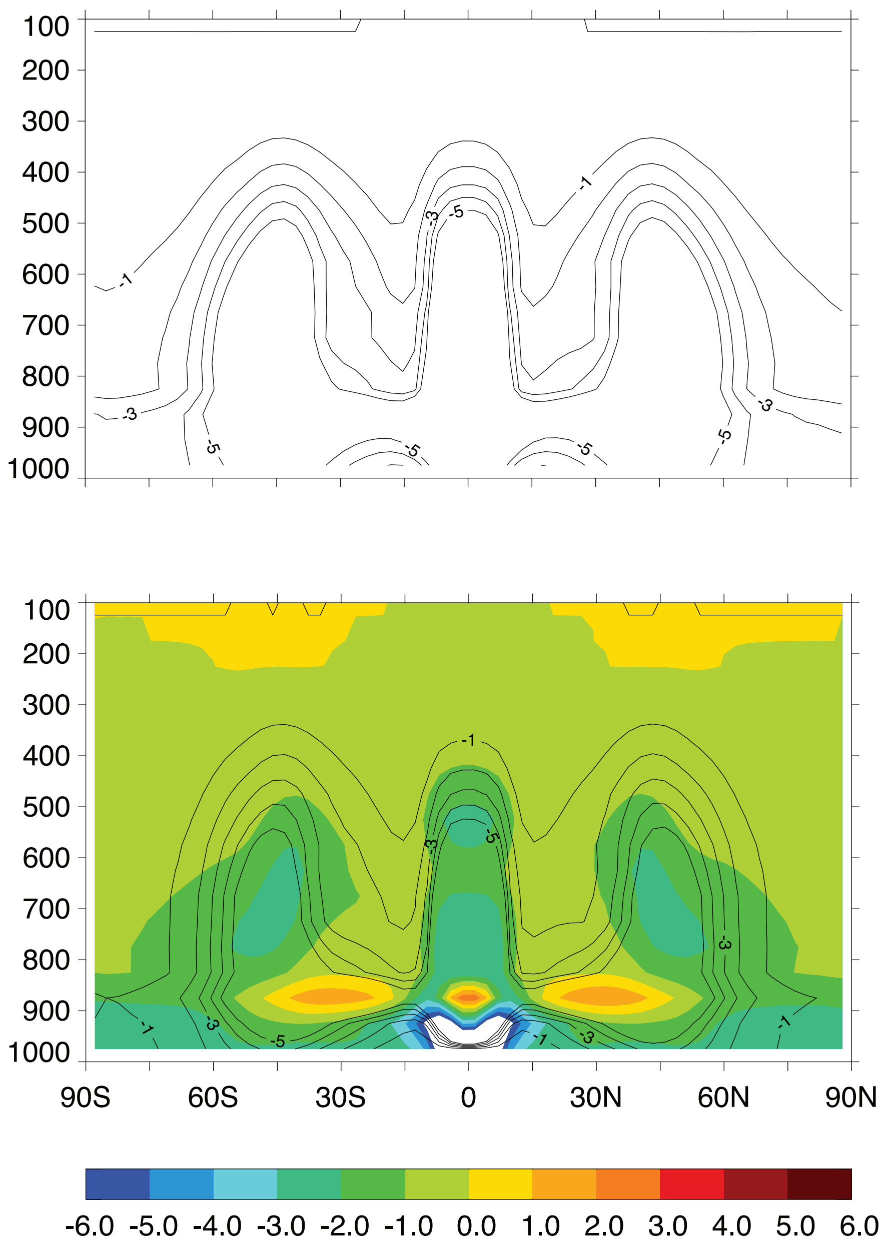

FIG. 3. Total water vapor tendency due to phase transition (not including evaporation) (10^{-9} kg kg^{-1} s^{-1}) in CNTL-C (contours in the upper panel) and in CNTL-SA (contours in the lower panel). The difference is shown in color shading in the lower panel. White in a colored figure indicates that values are outside the range of the color bar throughout the paper.

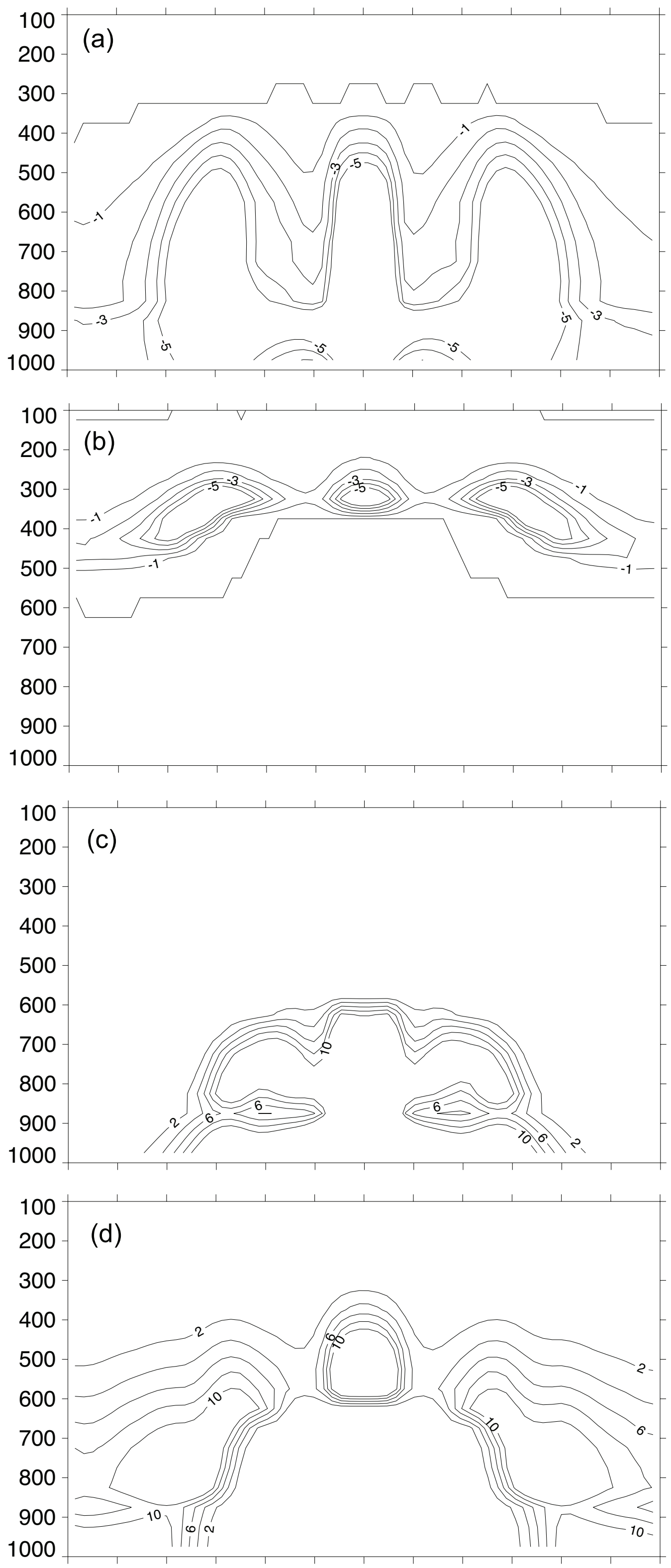

Fig. 4. Water vapor tendencies due to condensation (10^{-9} kg kg^{-1} s^{-1}) (a), ice deposition (10^{-10} kg kg^{-1} s^{-1}) (b), rain re-evaporation (10^{-10} kg kg^{-1} s^{-1}) (c) and snow sublimation (10^{-10} kg kg^{-1} s^{-1}) (d) in CNTL-C. Cloud liquid re-evaporation and ice sublimation are negligible.

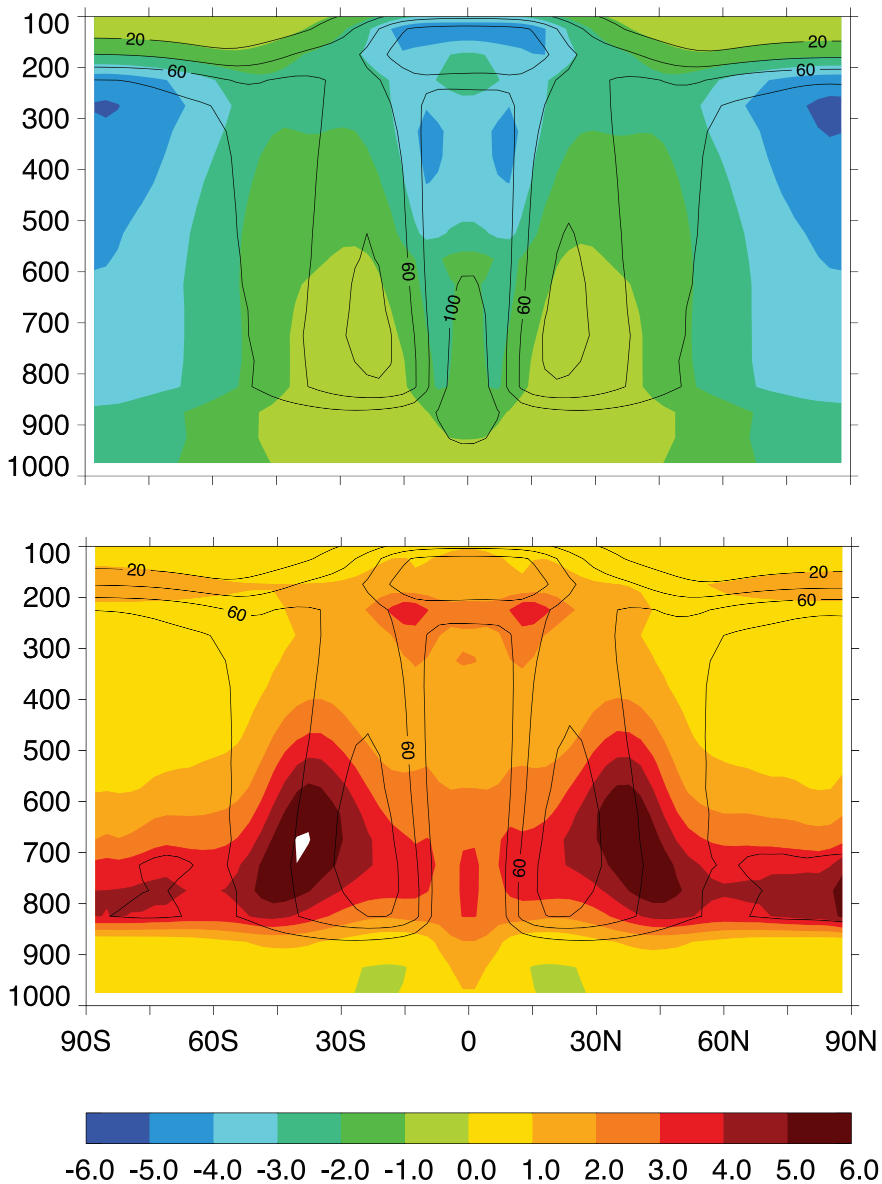

FIG. 5. RH difference (%) between CNTL-C and NW (color shading in the upper panel) and between NW and CNTL-SA (color shading in the bottom panel). The contours represent RH in NW (the upper panel) and in CNTL-SA (the lower panel).

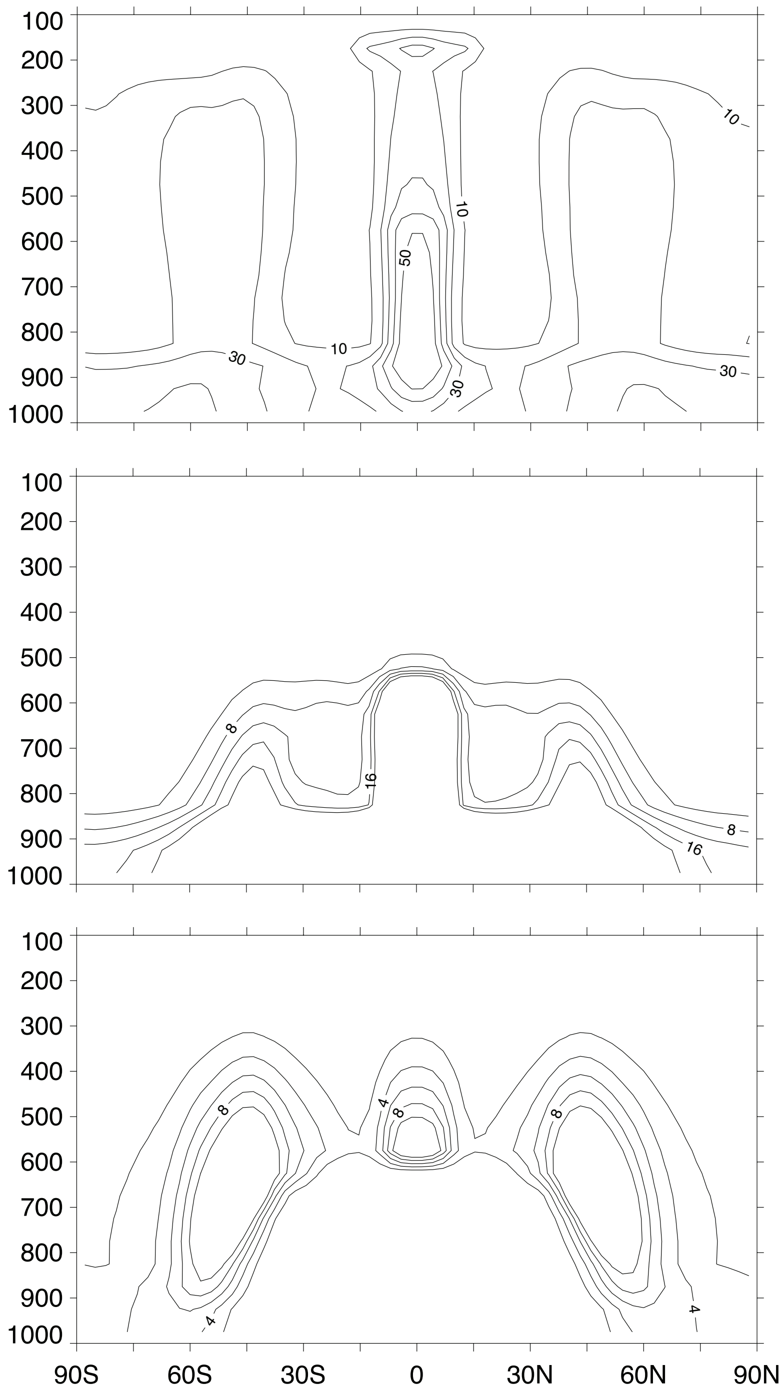

FIG. 6. Cloud fraction (%, the upper panel), liquid (10^{-6} kg kg^{-1}, the middle panel) and ice (10^{-6} kg kg^{-1}, the lower panel) in CNTL-C.

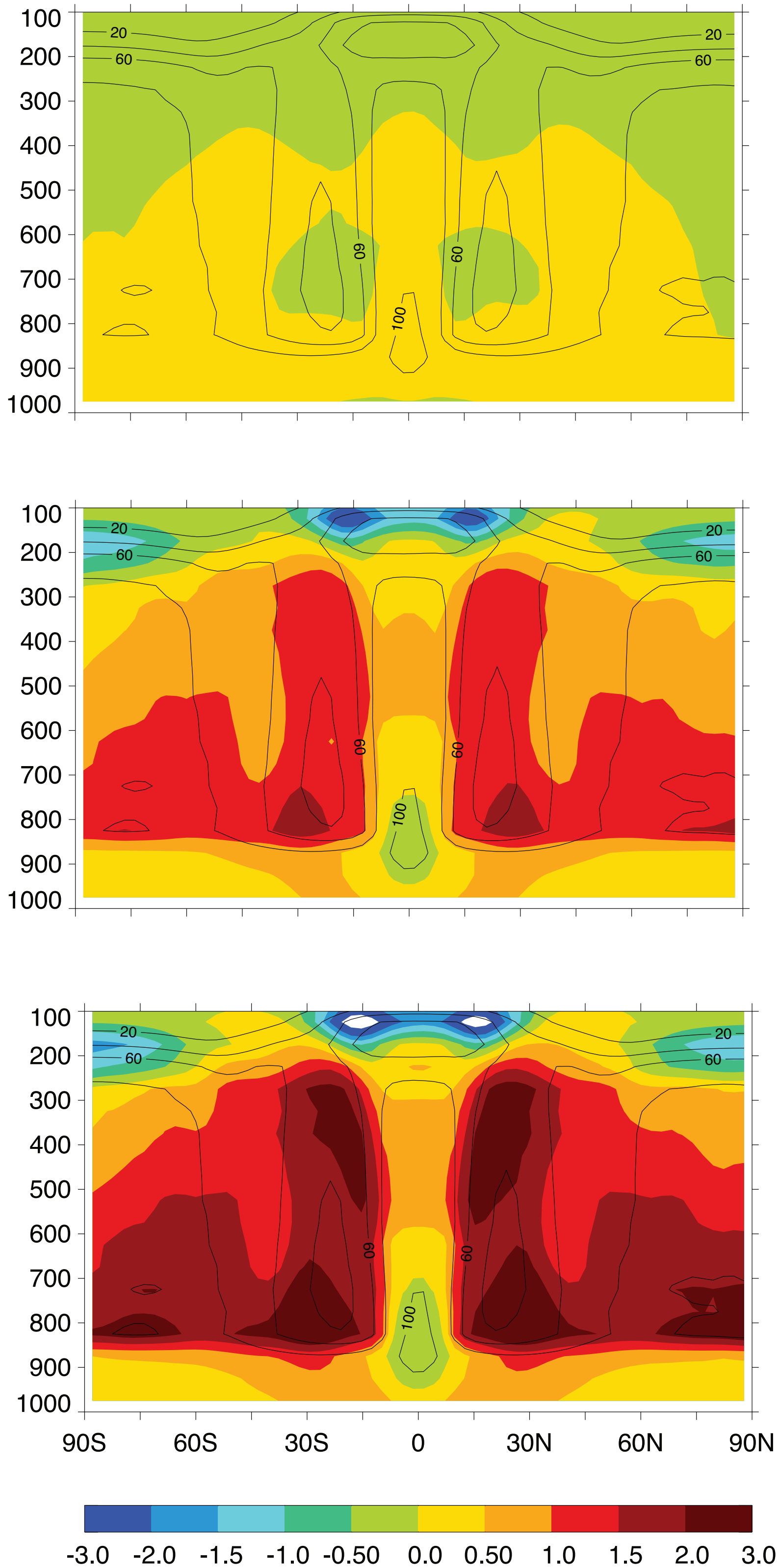

FIG. 7. RH difference (%) between UN and CNTL-C (the upper panel), between TS and CNTL-C (the middle panel) and between TC and CNTL-C (the lower panel). The contours represent RH in CNTL-C.

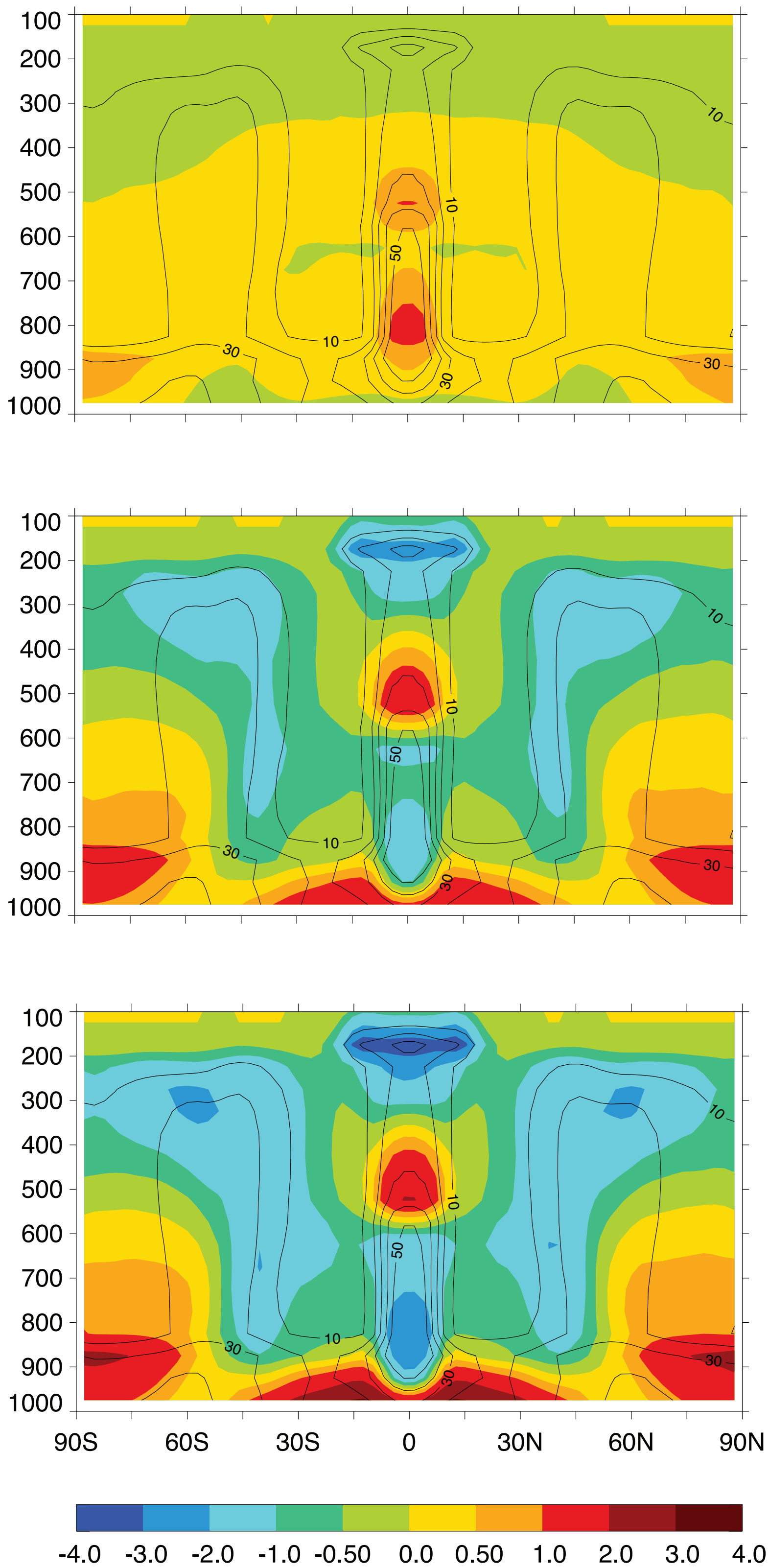

FIG. 8. Cloud fraction difference (%) between UN and CNTL-C (the upper panel), between TS and CNTL-C (the middle panel) and between TC and CNTL-C (the lower panel). The contours represent the cloud fraction in CNTL-C.

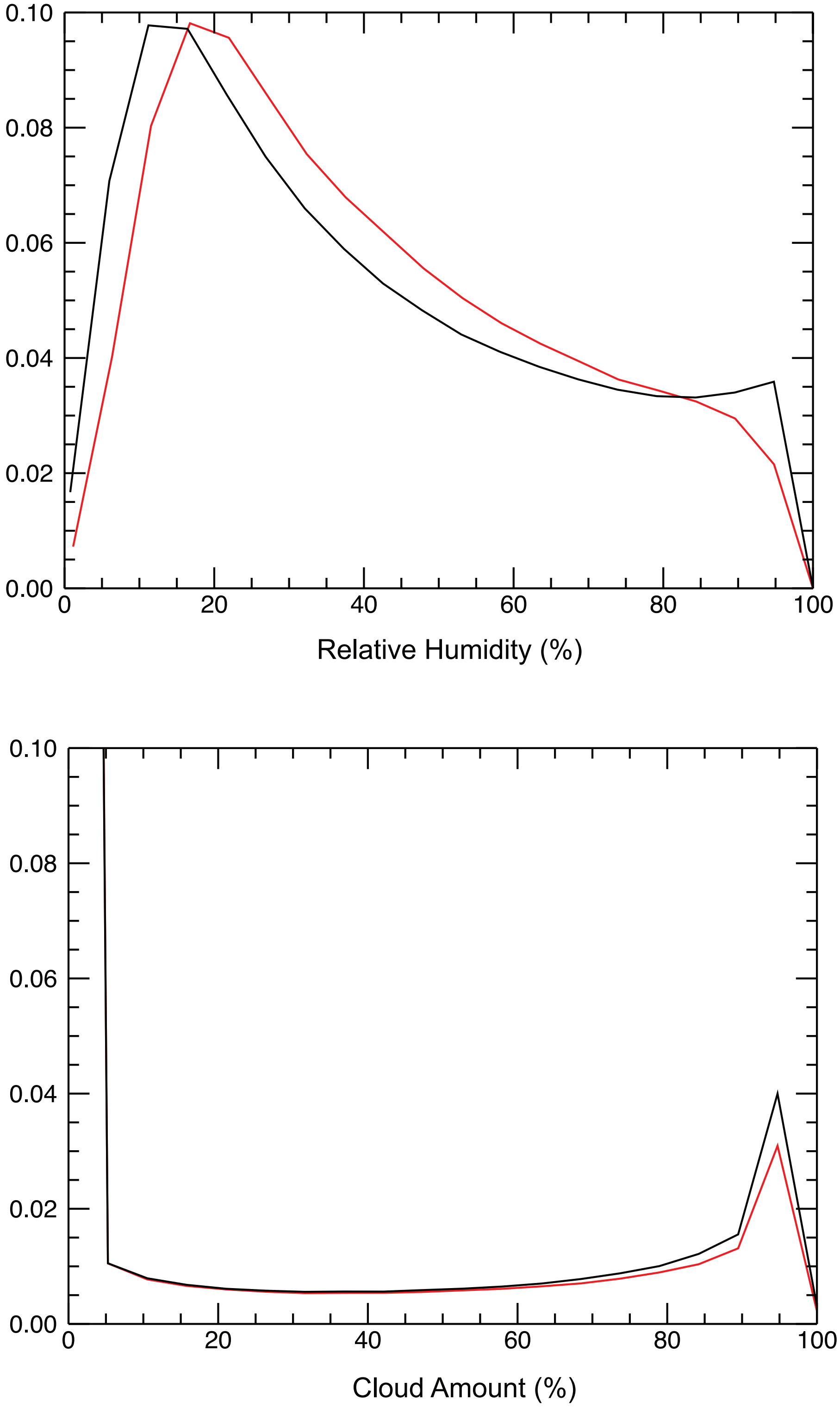

Fig. 9. Normalized histograms of 2-hourly RH (%) and cloud fraction (%) in a domain between 15° and 45°N and between 600 and 700 hPa.The 20 bins are of equal width (5%). The black and red lines represent CNTL-C and TC, respectively. Note that the y-axis of the lower panel is cut off at 0.1.

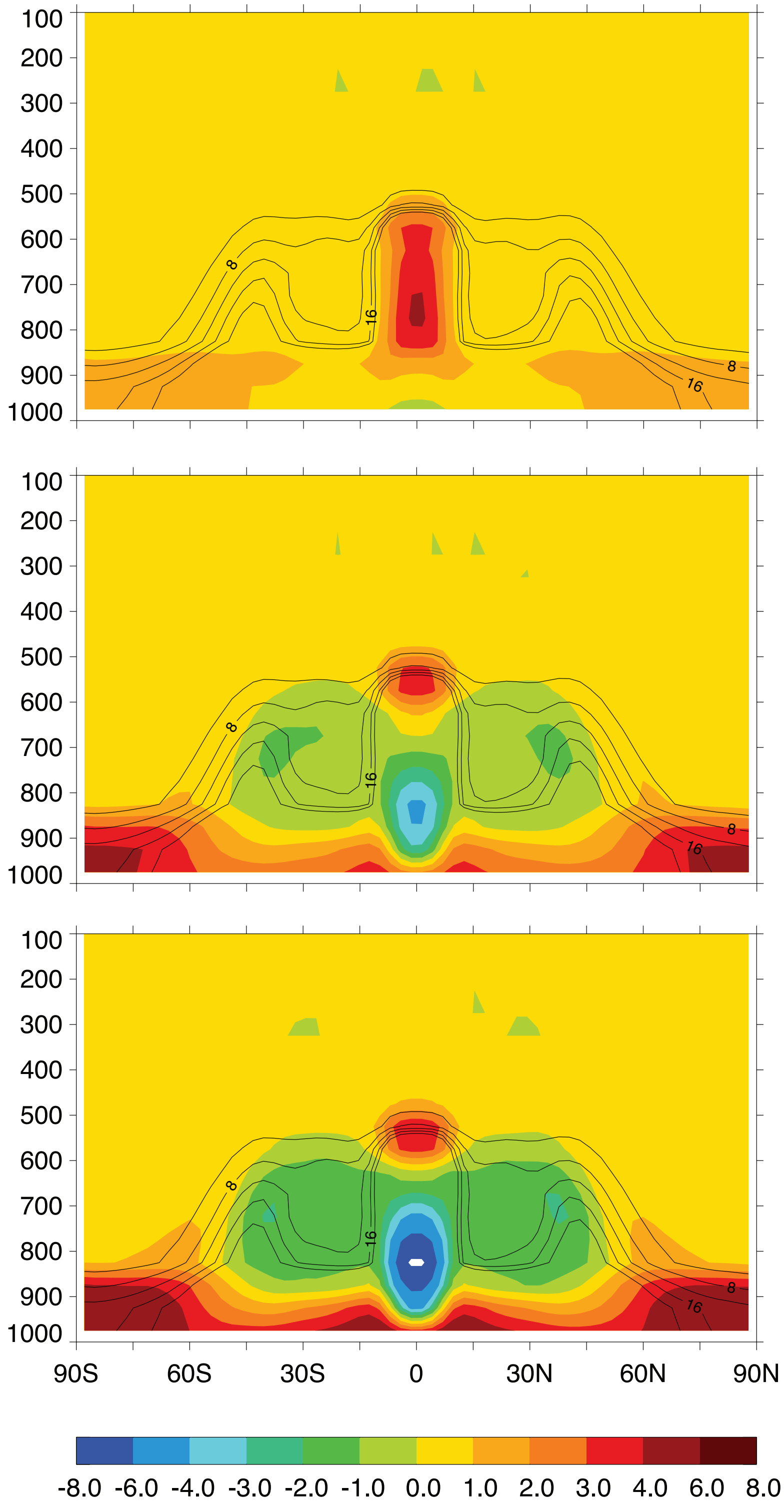

FIG. 10. Cloud liquid difference (10^{-6} kg kg^{-1}) between UN and CNTL-C (the upper panel), between TS and CNTL-C (the middle panel) and between TC and CNTL-C (the lower panel). The contours represent the cloud fraction in CNTL-C.

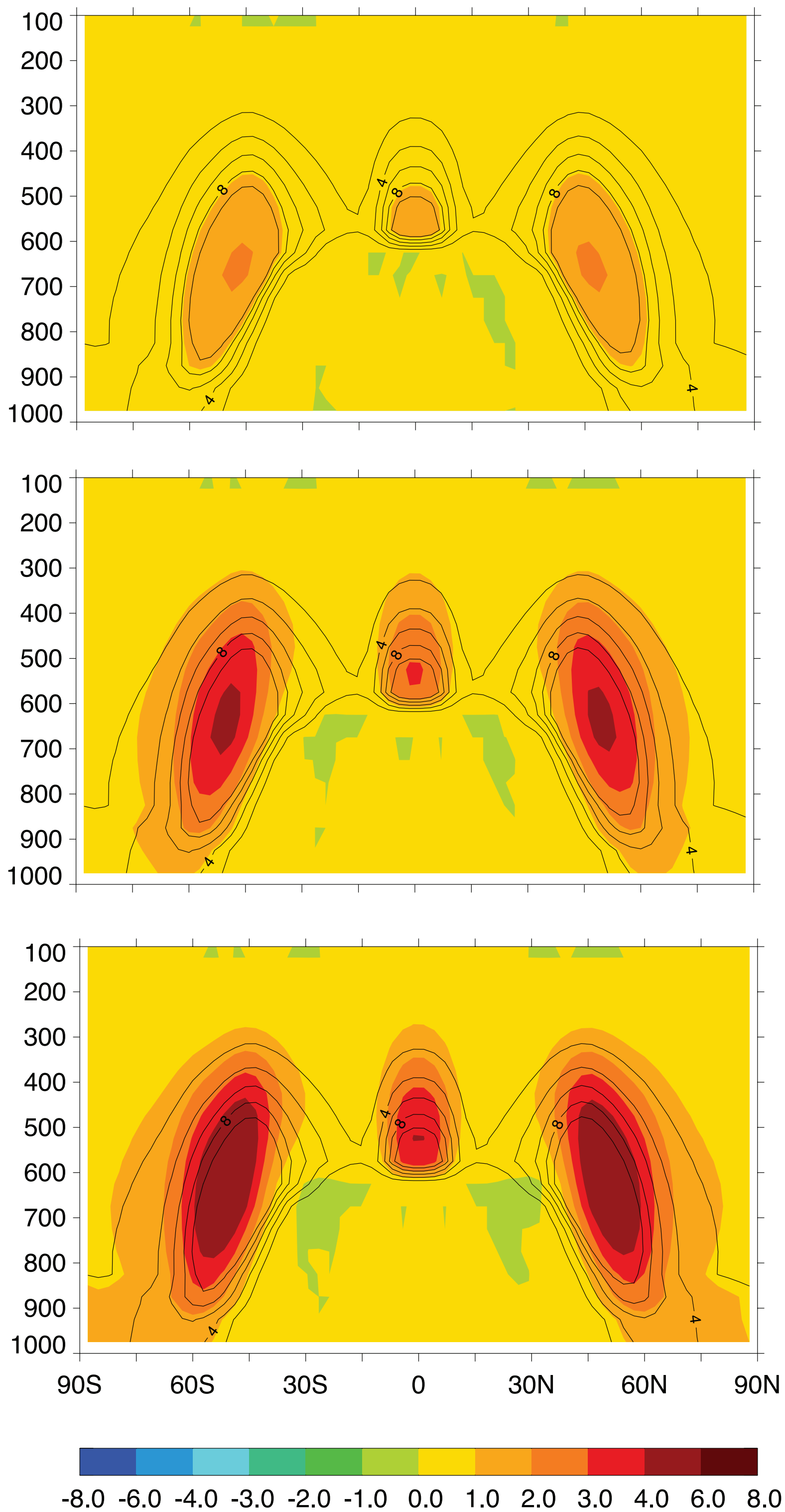

FIG. 11. Cloud ice difference (10^{-6} kg kg^{-1}) between UN and CNTL-C (the upper panel), between TS and CNTL-C (the middle panel) and between TC and CNTL-C (the lower panel). The contours represent the cloud fraction in CNTL-C.